Gb/s Visible Light Communications With Colloidal Quantum Dot Color Converters

Miguel F. Leitao, Joao M. M. Santos, Benoit Guilhabert, Scott Watson, Anthony E. Kelly, Mohamed S. Islim, *Student Member, IEEE*, Harald Haas, Martin D. Dawson, *Fellow, IEEE*, and Nicolas Laurand, *Member, IEEE*

***Abstract*—This paper reports the utilization of colloidal semiconductor quantum dots as color converters for Gb/s visible light communications. We briefly review the design and properties of colloidal quantum dots and discuss them in the context of fast color conversion of InGaN light sources, in particular in view of the effects of self-absorption. This is followed by a description of a CQD/polymer composite format of color converters. We show samples of such color-converting composite emitting at green, yellow/orange and red wavelengths, and combine these with a blue-emitting microsize LED to form hybrid sources for wireless visible light communication links. In this way data rates up to 1 Gb/s over distances of a few tens of centimeters have been demonstrated. Finally, we broaden the discussion by considering the possibility for wavelength division multiplexing as well as the use of alternative colloidal semiconductor nanocrystals.**

***Index Terms*—Visible light communications, colloidal quantum dots, semiconductor nanocrystal, GaN, LED, OFDM.**

I. Introduction

COLLOIDAL semiconductor quantum dots (CQDs) are efficient light-emitting nanoparticles that have been the focus of intense research and development over the last two decades [1], both in academia and in industry. While CQDs are finding use as fluorescent tags for bio-imaging and bio-assays [2], as light-emitting diode (LED) and laser gain materials [3]–[6], or again as light-harvesting elements in photovoltaics [7], their most important application in terms of volume to date is as phosphors in hybrid light-emitting devices and displays [8]–[10]. Thanks to their solution processability, high photoluminescence quantum yield (PLQY), broad absorption and narrow emission linewidths, CQDs are an attractive alternative to the rare-earth phosphors that are found in standard commercial white LEDs. In particular, their narrow emission linewidth enables the generation of colors with high purity, enhanced gamut (e.g. CQDs are found in the new generation of high-definition LCD screens) and superior white light quality for illumination [8], [9]. We will see in this paper that CQDs can also be utilized for data communication links at 1 Gb/s rates and above when hybridized with InGaN optical sources.

Our group is utilizing CQDs for color-converting blue/violet micro-size InGaN LEDs (μLEDs) [11], [12]. Such μLEDs have typical emitting active areas of between 10 and 10^3 μm^2, i.e. one to two orders of magnitude smaller than standard LEDs. These μLEDs can also be arranged in array-format with hundreds or thousands of pixels per mm^2 and can be integrated with CMOS electronics for spatial and temporal control, creating a microdisplay technology that can be used for different applications [13]–[15]. A monolithic μLED array is limited to one emission wavelength, set by the InGaN epitaxial structure, and the wavelength region where InGaN LED emission is the most efficient is in the blue/violet [16]. The solution-processability of CQDs gives flexibility in the fabrication of hybrid devices and we have demonstrated multi-color emission from a single μLED chip by selectively overcoating μLED pixels with CQD materials [11] – these absorb the μLED light and re-emit it at longer wavelengths. The μLEDs are also attractive sources for visible light communications (VLC), because their array formats enable spatial multiplexing and, crucially, because blue μLEDs can be modulated at high-speed [15], [17] with multi-Gb/s VLC links demonstrated [18].

VLC, and by extension LiFi [19], is a next generation communication technology seen as essential to help cope with the ever-increasing demand on wireless data communications [19]–[21]. It capitalizes on the rapid development of efficient blue InGaN-based LEDs and lasers, mainly driven by the needs of the solid-state lighting industry [20]. It is anticipated that VLC will transform light bulbs into the emitters of a new wireless communications network and enable systems to cope with the vast amount of data created by mobile applications and the Internet of Things [20]. One challenge is that efficient InGaN LEDs cannot cover the whole visible region or intrinsically

Manuscript received December 21, 2016; revised March 24, 2017; accepted March 28, 2017. This work was supported by the Engineering and Physical Sciences Research Council under Grant EP/K00042X/1. DOI for supporting data: 10.15129/54c94f1c-c62c-4b0c-9e90-256d5c2ac1ee. *(Corresponding Author: Nicolas Laurand.)*

M. F. Leitao, B. Guilhabert, M. D. Dawson, and N. Laurand are with the Department of Physics, Institute of Photonics, SUPA, University of Strathclyde, Glasgow G1 1XQ, U.K. (e-mail: miguel.leitao@strath.ac.uk; benoit.guilhabert@strath.ac.uk; m.dawson@strath.ac.uk; nicolas.laurand@strath.ac.uk).

J. M. M. Santos was with the University of Strathclyde, Glasgow G1 1XQ, U.K. He is now with ST Microelectronics, Edinburgh EH8 9YL, U.K. (e-mail: joao.santos@strath.ac.uk).

S. Watson and A. E Kelly are with the School of Engineering, University of Glasgow, Glasgow G12 8QQ, U.K. (e-mail: Scott.Watson@glasgow.ac.uk; Anthony.Kelly@glasgow.ac.uk).

M. S. Islim and H. Haas are with the LiFi Research and Development Centre, Institute for Digital Communications, University of Edinburgh, Edinburgh EH8 9YL, U.K. (e-mail:-mail: M.Islim@ed.ac.uk; h.haas@ed.ac.uk).

Color versions of one or more of the figures in this paper are available online at http://ieeexplore.ieee.org.

Digital Object Identifier 10.1109/JSTQE.2017.2690833

emit white light. Longer wavelengths and white light as used for lighting are obtained through color conversion whereby a rare-earth phosphor material overcoats a blue InGaN source. The approach is efficient but rare-earth phosphors have recombination lifetimes >1 μs, therefore the resulting sources cannot be modulated at high speed for data transmission, the bandwidth of white phosphor LEDs typically being less than 2 MHz [21]. Consequently, light converters with shorter photoluminescence lifetimes than rare-earth phosphors, meaning they can be modulated faster because modulation bandwidth and PL lifetime are inversely proportional, are needed [12]. As we will see, CQDs have typical PL lifetimes of tens of nanoseconds and are consequently intrinsically faster. In addition, the possibility to tailor the optical properties of CQDs through the design of heterostructures is appealing. The narrow emission linewidth of CQDs that was mentioned above as a parameter for superior color purity and light quality, is also attractive for wavelength division multiplexing, whereby data is sent in parallel using different colours. The latter is particularly desirable for waveguide-based VLC, as is for example used in-vehicle communication systems.

In this paper, we show that CQDs can indeed form high performance color converters for VLC. In Section II, we review some basics on CQDs, including the main material composition and structure designs for visible emission, and the important optical characteristics for VLC. We also discuss the effect of self-absorption on the static and dynamic properties of the color converters. In Section III, we present a CQD composite format of color converter and its characteristics. We relate results to the discussion of Section II. In Section IV, we report the demonstration of VLC using CQD color converters and show that a >1 Gb/s data link can readily be achieved. Orthogonal frequency division multiplexing (OFDM), a multiple carrier modulation scheme, is used here to maximise the utilization of the bandwidth of the CQD-converted optical source. Section V gives an outlook for future development of the technology and finally Section VI summarizes the paper.

II. CQDs for Light Conversion

In this paper, we are overviewing CQDs for light conversion of InGaN μLEDs to create sources for VLC. In that context, the CQD material is overlaid on top of a μLED device as shown in Fig. 1(a). The CQD material absorbs the light emitted by the μLED and re-emits photons at longer wavelengths. It is possible to emit at different wavelengths across the visible spectrum through the choice of the CQD material. In this paper, we are focusing on single-wavelength CQD-converted μLEDs and analyse their performance for VLC although such a hybrid LED structure can also generate white light, e.g. for illumination, through color mixing by combining partially absorbing CQD structures emitting at a few different wavelengths. For VLC, the μLED is modulated with encoded data, the μLED light acting as the primary carrier. Thanks to the color converting CQDs, the data is transferred to a longer wavelength carrier – the light emitted by the CQDs. In this section, after describing basics of CQDs, we discuss with the help of a simple, qualitative model for self-absorption the guidelines for the design of CQD color converters for VLC.

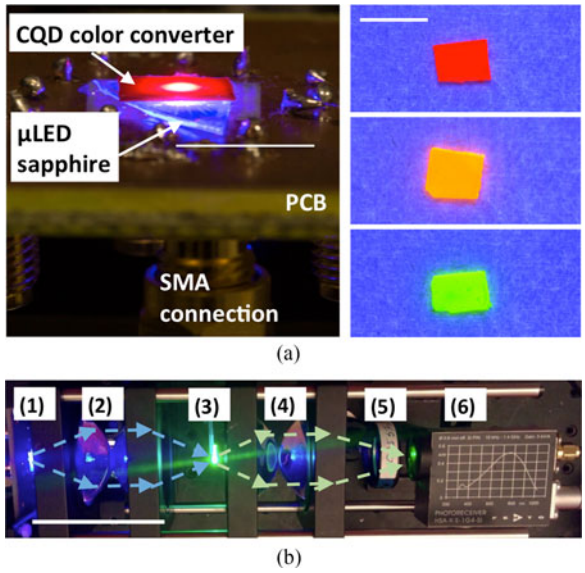

Fig. 1. (a) On the left, image of a hybrid μLED with a red CQD color converter on top of the μLED sapphire substrate. On the right, images of red, yellow/orange and green CQD/PMMA color converters under UV illumination. The white scale lines represent 1 cm. (b) The remote excitation set-up used for the color converter characterization prior to integration with the μLED. (1) is the μLED array with one pixel on; (2) is a set of lenses to collect and image the μLED emission onto the color converter sample (3); (4) is an identical set of lenses to collect the converted emission and image it onto the detector (6). A filter (5) can be placed before the detection. Different detection instruments are used for the optical power, bandwidth and optical spectrum measurements. The scale bar represents 5 cm. The VLC data link set-up is similar except that the CQD color converter is then in direct contact with the μLED sapphire substrate as in (a) and only one set of optics is used.

A. Materials, Structures and Optical Properties

The types of CQDs we discuss here are core/shell heterostructures [22] with typical diameter below 10 nm. The role of the shell material is to passivate the surface of the CQD core, enabling high PLQY. It also allows for engineering of the excitonics, referring to the way the electrons and holes are confined within the CQD heterostructure and how their respective wavefunctions overlap. Type I CQDs have strong overlap because both holes and electrons are primarily confined in the core. The overlap in type II CQDs is reduced because the electron and hole are spatially separated, one type of carrier being mostly confined in the core while the other is mostly confined in the shell. Quasi-type II represents the intermediate case where one type of carrier is confined in the core while the other is delocalized over the whole heterostructure. Excitonics directly dictates the optical properties of CQDs and their dynamics and is therefore important for color conversion and VLC. A priori, type I CQDs are desired because a strong electron/hole overlap translates into an increased radiative recombination rate of the exciton and hence to a reduced PL decay time.

CQDs can be formed with many different II-VI, IV-VI, I-VII and III-V semiconductor alloys and even with group IV materials like silicon. The most mature materials are based on

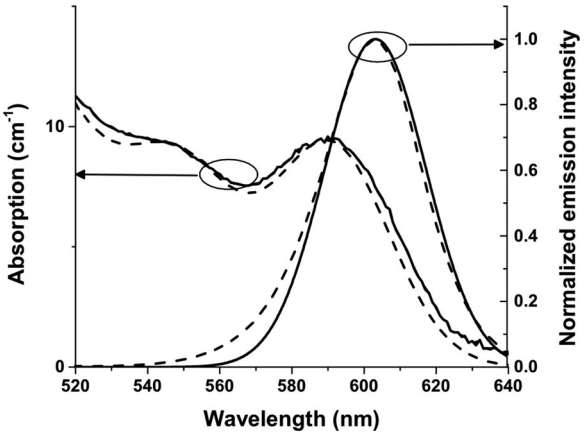

Fig. 2. Absorption and normalized emission intensity of CdSe/ZnS quantum dots – data (dashed lines) and model (full lines).

CdS, CdSe, ZnS, InP and PbS and enable coverage of the visible and near-infra-red range of the spectrum. In this paper, we are concerned with heterostructures made from CdSe, CdS and ZnS, with ZnS being the outer shell material.

At energy above their first excitonic transition, the absorption of CQDs continuously increases as can be seen in Fig. 2 for typical CdSe/ZnS CQDs. For information, this absorption measurement is based on [11] where the CQDs were diluted in an epoxy resin. The plot shows the two first, well-defined exciton absorption lines. The continuous increase in absorption at decreasing wavelengths comes from the multiplicity of higher energy transitions. In practice, this broad absorption spectrum simplifies the implementation of color conversion. Emission linewidths at full width at half maximum (FWHM) of 30 nm are typical for an ensemble of CdSe/ZnS CQDs (see Fig. 2). This relatively narrow emission linewidth makes CQDs superior to rare-earth phosphors and light-emitting organic materials for generating colors of high purity with high efficiency. As stated before, a narrow emission linewidth is also attractive for the future implementation of wavelength division multiplexing scheme in VLC systems, whereby data streams are sent in parallel using carriers at different colors.

An important parameter for VLC is how fast the color converter can respond to optical modulation. This speed is directly linked to the PL lifetime, which is a measure of how fast an exciton is formed by absorption of a photon or how fast it recombines, either radiatively or non-radiatively. In the ideal case where non-radiative recombination is negligible (so that the PLQY is maximized) it is the radiative lifetime that dictates the PL lifetime. The fine structure of the exciton ground state levels in most III-V CQDs leads to a PL that is the result of the recombination of excitons that are Bolzmann-distributed over a dark state (forbidden transition with >1 μs lifetime) and a bright state (allowed transitions with ns lifetime) [22]–[24]. As a result, at room temperature, typical PL lifetimes in type I and quasi-type II CQDs are on the order of 10 ns to a few tens of ns, i.e. slower than in semiconductor quantum wells but still several orders of magnitude shorter than in phosphors. Surface states can also slow down the emission of photons and is the origin of a long-lived tail in the PL lifetime measurements of certain CQDs, but the overall effect on the mean PL lifetime is minimal in high PLQY CQDs.

B. Self-Absorption Effects

CQDs, especially type I CQDs, have a limited Stokes shift, which results in the emission spectrally overlapping the absorption and in turn leads to a non-negligible probability for self-absorption. Self-absorption affects both the static and dynamic properties of the color converters. To understand how, we consider typical type I CdSe/ZnS CQDs with PL and absorption spectra as shown in Fig. 2. The intrinsic PL of the CQDs overlaps with the absorption spectrum. The dashed curves in Fig. 2 are theoretical functions that model the spectral data. We used a single Gaussian function ($\lambda = 603.5$ nm and 28 nm FWHM) for the emission and three Gaussians with different contribution strength for the absorption (respectively 30% $\lambda_1 = 591$ nm with 32 nm FWHM; 30% $\lambda_2 = 547$ nm with 34 nm FWHM; 40% $\lambda_3 = 507$ nm with 32 nm FWHM). The origin of the 3 Gaussians can be ascribed to different transitions in the spectral range considered. The model functions overlay the data relatively well over this spectral range as can be seen in Fig. 2. We then use these model functions to explore qualitatively the effect of self-absorption on the properties of a CQD color converter.

Because of the limited Stokes shift, a photon emitted by a CQD can be reabsorbed as it travels within the CQD color-converting structure. An exciton created through such a self-absorption event has a certain probability, given by the PLQY, to recombine by emitting another PL photon. This cycle of self-absorption/emission can repeat itself as the emitted photons interact with the CQDs. While a full quantitative study of the problem requires a numerical analysis, we can get useful insights into the process with a simplified approach [25]. For this, we make a number of assumptions as explained in [25]: the optical path length of all photons is equivalent and we consider exactly one self-absorption and re-emission cycle. In such a case, the spectral emission *I(λ,z)* of the color converter is given by:

$$I(\lambda, z) = S(\lambda, z) \cdot \left(1 + \int_{\lambda} \alpha(\lambda) \cdot QY \cdot E_{\text{int}}(\lambda) d\lambda\right) - (1 - \exp(-\alpha(\lambda) z)) \cdot S(\lambda, z) \quad \text{(1-a)}$$

$$S(\lambda, z) = QY \cdot E_{\text{int}}(\lambda) \cdot P(z) \quad \text{(1-b)}$$

$$P(z) \propto 1 - \exp(-\alpha_P z) \quad \text{(1-c)}$$

In (1-a)–(1-c) z is the spatial position, i.e. the path length for the photons in the color converter. If we look at the hybrid LED of Fig. 1(a), the position $z = 0$ is the interface between the μLED sapphire substrate and the color-converter. *S(λ,z)* is a source term that depends on the intrinsic, normalized CQD spectral emission $E_{\text{int}}(\lambda)$; QY is the PLQY taken here arbitrarily as 0.7; *P(z)* is a term proportional to the pump excitation (μLED) absorbed with a dependence on z for taking into account the pump depletion; $\alpha(\lambda)$ is spectral absorption, the magnitude of which depends on the concentration of CQDs; and α_P is the absorption term of the excitation pump equal here to 25 cm^{-1}.

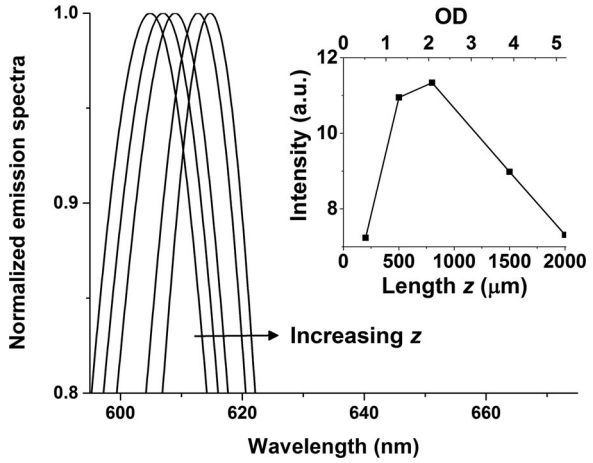

Fig. 3. Normalized emission spectra for increasing length scale z of the CQD converter with a red-shift caused by self-absorption. Inset: Corresponding integrated emission intensity.

What (1-a) describes is the evolution of the color converter spectral emission intensity, *I(λ,z),* as its length z increases. Because of the simplifications made, the approach underestimates the effects of self-absorption and serves here to illustrate these effects qualitatively.

Fig. 3 plots the normalized emission spectrum of such CQDs for different lengths of color converter z, respectively 200 μm, 500 μm, 800 μm, 1500 μm and 2000 μm. In this range, the peak wavelength of the CQD converter linearly red-shifts as a function of z. The shift going from a 25 μm thickness to a 700 μm thickness is 10 nm. Note that such a shift would also be present for a fixed z if one were to increase the CQD concentration because the spectral absorption depends on the cross-section and the concentration of CQDs. Although it is to be noted that for high concentration levels non-radiative energy transfer processes between CQDs can also contribute to the spectral shift, we consider here CQD concentration levels below a few % in volume ratio where self-absorption is the dominant effect. This is justified because the mean distance between CQDs, considering ideal dispersion in the matrix, is between 20 nm and 40 nm [26]. The inset of Fig. 3 shows the integrated intensity emitted by the color converter made of this material at different values of z (bottom x-axis giving the values of z). The top x-axis represents the optical depth, noted OD, of the color converter at the pump wavelength, i.e. OD $= \alpha_P z$ is the natural logarithm of the ratio of incident to transmitted pump power. OD is a useful parameter to compare color-converters made of different materials or of different CQD concentration, hence having different values of α_P, as it is directly related to the amount of absorbed pump power (the pump being the light to be converted). We utilize OD again in Section III for the experimental characterization of CQD color converters. Initially, the emission increases as z (and OD) increases but saturation, caused by depletion of the excitation pump and absorption/re-emission of photons with a limited QY, is reached between 500 and 1000 μm. Past this point, for increasing length the emitted intensity actually decreases. There is therefore an optimum thickness of the color converter (for a given CQD concentration) to achieve maximum conversion. These self-absorption effects on the emission spectrum and converted intensity of the color converter are in fact common to most light-emitting materials including phosphors and can be taken into account for optimization. Although self-absorption can be suppressed in type II CQDs with high Stokes shifts, these CQDs have longer PL lifetime and are not suitable for VLC.

The process of self-absorption also increases the PL lifetime of the color-converting structure [27]. We consider a color-converter in slab format made of the same CQD material as previously. One face of the slab represents the output. The thickness of the slab is *L*. A photon of wavelength λ emitted at a distance z from the output and propagating at an angle θ from the normal to the output interface has a probability p_a of being absorbed, given by:

$$p_a(\lambda) = 1 - \exp\left(-\frac{\alpha(\lambda)\cdot z}{\cos\theta}\right) \tag{2}$$

In (2), for simplification we have made the approximation that all photons reaching the output interface at an angle θ smaller than the critical angle θ_c of the color converter/air interface (here taken as 45°) escape the structure [27]. Then, the net fraction, *F(λ,L)*, of photons at wavelength λ emitted in the CQD converter that are re-absorbed is found by:

$$F(\lambda, L) = \frac{1}{L\cdot\theta_c}\int_{\theta<\theta_c}\int_0^L p_a(\lambda, z)dzd\theta \tag{3}$$

Finally, Φ the fractional increase in the PL lifetime due to self-absorption, and in turn the decrease in the modulation bandwidth BW_{ratio}, are obtained with (4-a) and (4-c).

$$\Phi = \frac{1}{1 - F(\lambda, L)} \tag{4-a}$$

$$\tau = \frac{\sqrt{3}}{2\cdot BW} \tag{4-b}$$

$$BW_{\text{ratio}} \propto 1/\Phi \tag{4-c}$$

Equation (4-b) gives the relation between the average PL lifetime, τ, and the modulation bandwidth, *BW*, defined as the frequency at which the modulated optical power is half its DC value. Fig. 4 plots both Φ and BW_{ratio} as a function of the color converter length *L* made with the CQD material of Fig. 2 (QY of 70%). For a 3mm-thick color-converter the PL lifetime is increased by more than 100% and the modulation bandwidth decreased by 50%. At 800 μm thick, corresponding to the calculated optimum length for conversion (see inset Fig. 3), this increase is around 25%, corresponding to a decrease in the modulation bandwidth of 20%. To minimize this self-absorption, the length of the color-converter should be minimized. Doing this while maintaining efficient color-conversion means exciting the CQDs with a pump at a shorter wavelength, where absorption is higher. For InGaN-based sources for VLC, this could be done by using UV-violet LED, e.g. at 370 nm. However, the most efficient InGaN LEDs emit in the blue/violet (400–450 nm) so there is a trade-off to consider.

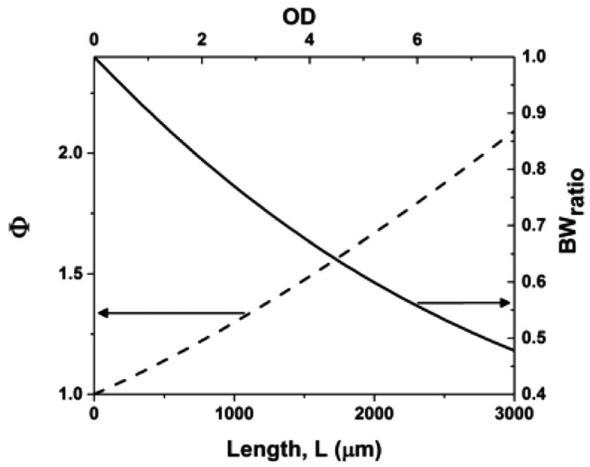

Fig. 4. Lengthening of the PL lifetime as a function of the color converter length, L, (dashed curve) and corresponding decrease in the optical modulation bandwidth (full curve).

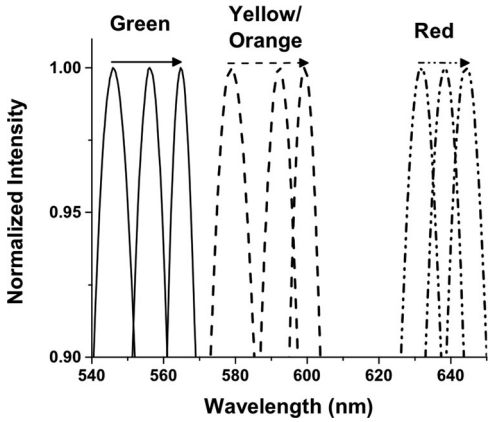

Fig. 5. Optical spectra of the color converters – the arrow indicates increasing CQD concentration, hence increasing OD (here from 1.9 to 5.5) and self-absorption.

III. Color Converter Formats

In the following, we describe the fabrication and experimental characterization of color-converting slabs made of a CQD/Polymethyl methacrylate (PMMA) composite. Color conversion of a 450 nm μLED into 3 different wavelength regions (green, yellow/orange and red) is demonstrated. The effect of the CQD concentration on the converted light properties is shown and related to the discussion of Section II.

A. CQD Composite and Characterization

The CQDs used in this work are alloyed-core/shell CdSSe/ZnS nanocrystals with a 6 nm mean diameter. Engineering of the energy levels in such CQDs is obtained by changing the alloy composition of the core. These CQDs are basically type I although at shorter wavelengths, as the S/Se ratio is higher, the electron is less strongly localized in the core [22] and the type I character is less marked. The CQDs are initially in toluene solution. The toluene is evaporated and the appropriate weight of CQDs is mixed with PMMA. Samples with weight ratios of CQDs to PMMA between 1% and 10% are made, corresponding to CQD/PMMA volume ratios below 2%. Toluene is added and the CQD/PMMA solution is then stirred for approximately 15 hours. Slabs between 350 μm and 1 mm in thickness are fabricated by pouring the CQD/PMMA composite onto a PDMS mold and drying at room temperature. Once solidified, the CQD/PMMA slabs are removed from the mold. Fig. 1(a) shows examples of these color-converting slabs under illumination. A red color-converting slab sitting on a μLED is also shown.

For characterization of the pump (μLED light) absorption and of the color-converted emission spectrum, power and modulation bandwidth, a color-converter is remotely excited by a single μLED pixel from a μLED array as shown in Fig. 1(b). The array consists of 450 nm emitting square pixels, each with 100 μm x 100 μm emitting areas [28]. A single pixel has a turn-on voltage of 3.3 V and emits 8 mW (light directed forward) at a 200 mA injection current. The different color-converter samples are categorized by their color (green, yellow/orange and red) and by their absorption of the μLED light (OD, see Section II).

For modulation bandwidth measurements the μLED is driven by a DC-bias and a modulated small signal that is swept in frequency (combined with a bias T). The emission from the color-converter is detected by a fast photoreceiver (Femto HAS-X-S-1G4-SI, bandwidth up to 1.4 GHz). A network analyzer is utilized to both generate the modulated signal and record the detected frequency response. The modulation bandwidth is here defined as *BW*. In the following, we discuss the modulation bandwidth of the CQD color-converter and thereby unabsorbed and scattered blue LED light is filtered out before detection. The modulation bandwidth of the μLED is injection current dependent [15] and consequently so is the measured bandwidth of the color-converter. At an injection current of 200 mA the μLED bandwidth is 120 MHz.

B. Results and Discussion

Fig. 5 plots the typical normalized emission spectrum of the green, yellow/orange and red CQD color converters for a few OD values. These are, respectively, 1.9, 3.5 and 4.8 for the green CQDs; 2.4, 4.5 and 5 for the yellow/orange CQDs; 2, 4.5 and 5.5 for the red CQDs. The emission peak is seen to red-shift for increasing OD as is expected in a medium with self-absorption (see Section II).

Fig. 6(a) plots the measured color-converted optical power versus the pump power for green CQD samples with different OD values. For all samples, the color-converted power linearly increases with the pump indicating that there is no saturation even for the sample with the lowest OD. The highest converted power (0.8 mW) is obtained for an OD of 3.5, which corresponds to a μLED light absorption of 97%. At lower OD, the converted power is lower simply because the samples absorbed less blue μLED light. However, for OD above 3.5, the converted power decreases. Too high an OD is detrimental to the efficiency as was seen in Section II because of a combination of self-absorption of the PL and of depletion of the pump. It should

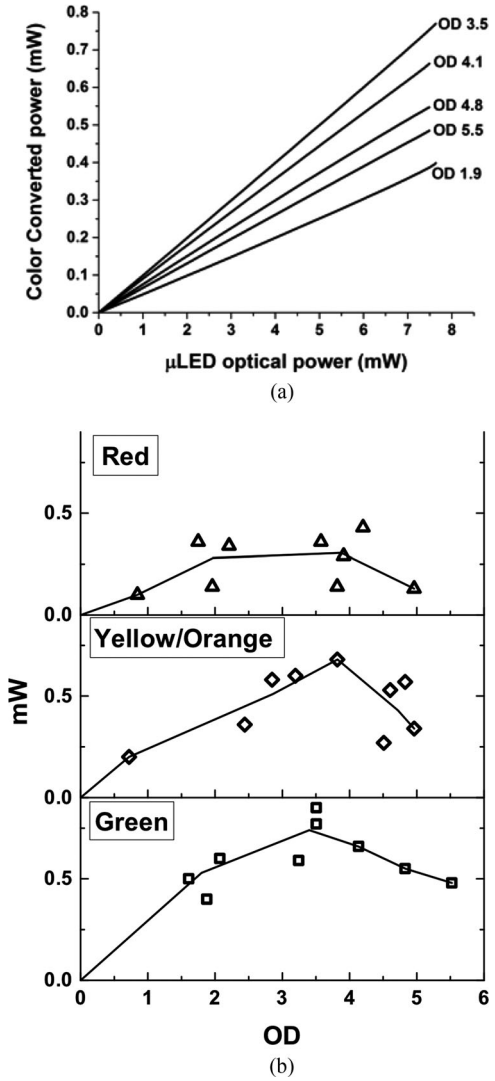

Fig. 6. (a) Color-converted optical power as a function of the excitation power for green CQD/PMMA color-converter with different pump absorption levels, indicated by the optical depth (OD) at the pump wavelength; (b) Color-converted power versus OD for the Green, Yellow/Orange and Red CQD composites.

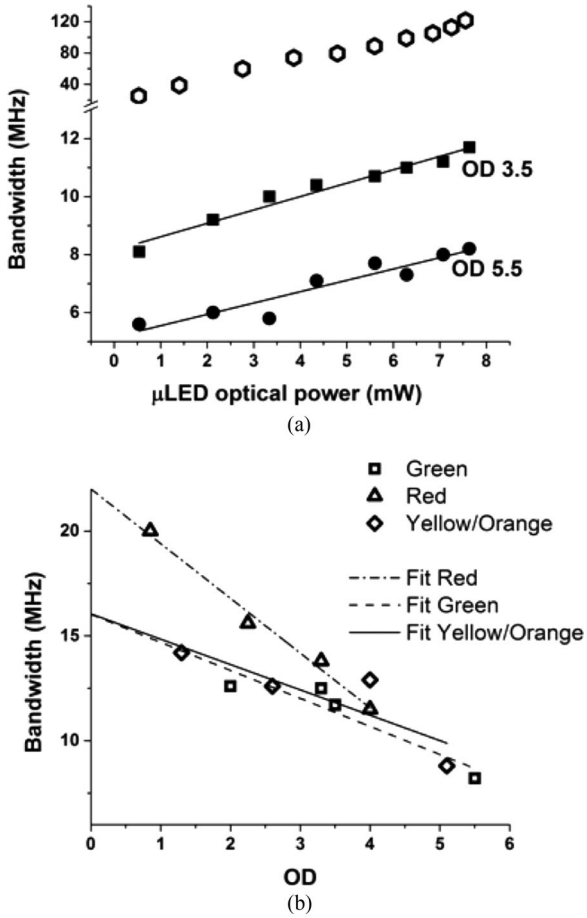

Fig. 7. (a) Bandwidth versus the μLED optical power for the green CQD/PMMA color converter with OD 3.5 (full squares) and OD 5.5 (full circles), and the μLED (open diamond). Please note the break in the y-axis and the change of scale for the μLED bandwidth data. (b) Bandwidth versus OD for green, yellow/orange and red CQD/PMMA color converters.

be noted that the optimum value of OD is here higher than that calculated in Section II. This is because the CQDs used in our experimental work are not identical to those considered in the previous section and the analytical model of Section II is only valid for qualitative discussions because it underestimates the strength of self-absorption in the color-converters.

The color-converted power at a μLED power of 8 mW is plotted as function of OD in Fig. 6(b) for green, yellow/orange and red CQD samples. The black lines are a guide for the eye drawn by linking average points in different OD windows; 0.5/1.5, 1.5/2.5, 2.5/3.5 etc. For all colors, the trend is the same. The color-converted power increases with OD up to an optimum value and then decreases at higher OD. The OD region for maximum converted power is for all colors between 3 and 4. The red CQDs are less efficient however, with a maximum output power below 0.5 mW. The reasons for this are still under investigation but a possible explanation is that the lattice mismatch at the core/shell interface in the red CQDs is higher than for both the yellow/orange and the green CQDs. In turn, the proportion of red CQDs with defects is higher and the PLQY lower.

Finally, the effect of self-absorption on the modulation bandwidth of the color converters is also evidenced experimentally. Fig 7(a) represents the optical bandwidth versus the bias pump power for the green color converter at two OD values, 3.5 and 5.5. In both cases the bandwidth increases linearly with the μLED optical power. This increase is mainly caused by the dependence of the μLED bandwidth on its injection current, and hence its output power, as shown also in Fig. 7(a) (please note the break in the y-axis). Further work is needed to study this behavior in detail but initial measurements on similar CQD/PMMA samples indicate that the increase in bandwidth with the excitation power is not intrinsic to the CQDs, at least not on this range of excitation power. The modulation bandwidth for the sample at OD 5.5, reaching 8 MHz at a pump power of 8 mW, is consistently lower than for the sample with OD 3.5, which reaches up to 11.5 MHz.

Because the value of the bandwidth of the μLED reaches 120 MHz at an 8 mW output power, i.e. around 10 times that

of the value measured for the color converters, the latter is close to the intrinsic color converter modulation bandwidth at this excitation power. Fig. 7(b) plots the modulation bandwidth at such a μLED bias optical power for different samples of green, yellow/orange and red CQD color converters. The lines are linear fits of the data, showing the trend of decreasing bandwidth versus OD. By extrapolation, the decrease between an OD of 0 (the 'idealized' intrinsic modulation bandwidth with no self-absorption) and an OD of 4 is between 25% and 40%, which is consistent with the simulation of Fig. 4 in Section II – some differences are expected because the effect depends on the wavelength and on the type of CQDs. The red CQD converters have the highest modulation bandwidth, up to 22 MHz at low OD, while the yellow/orange and green CQD converters have a similar extrapolated bandwidth at low OD, around 16 MHz. The corresponding PL decay lifetime, τ, as given by (4-b) is between 12.5 ns and 18 ns. At the OD of 3.5 for maximum converted power, the bandwidth for the green and yellow/orange, and the red CQDs are close to, respectively, 11.5 MHz and 13 MHz. We attribute the higher modulation bandwidth of the red CQDs to two things: a stronger type I characteristics with a stronger exciton overlap, hence faster radiative lifetime; and higher core/shell interfacial strain accelerating non-radiative recombination.

These experiments confirm what was discussed in Section II. A color-converted LED using a converting material with a non-negligible self-absorption creates a trade-off between converted power and modulation bandwidth. Often the power is as, or more, important than the bandwidth, e.g. a data link capacity is dependent on both the bandwidth and the received optical power. In some cases, a given converted power is needed for functions other than sending data, e.g. for display or illumination. But for VLC, the color-converter should not be designed to operate above the OD for maximum optical power because too high an OD will degrade both the power and the bandwidth. Exciting the CQDs at a wavelength where their absorption is stronger, i.e. typically at a lower wavelength, so that the optimum OD is attained for a lower color converter thickness or CQD concentration would minimize the effect of self-absorption. Obviously, the performance of InGaN LEDs decreases at wavelengths below 400 nm. Currently, a possible practical solution is to utilize 370 nm or even 400 nm emitting LEDs [29]. The performance of such CQD-converted LEDs for VLC is still to be explored.

IV. High-Speed VLC Demonstrations

In Section III, we have designed CQD/PMMA color converters with modulation bandwidth between 11 and 15 MHz at an OD for optimum color conversion. Such modulation bandwidths are at least an order of magnitude higher than for color converters made of rare-earth phosphors. In this section, CQD/PMMA converters are directly integrated on the sapphire surface of the μLED array as can be seen in Fig. 1(a) and used for VLC. It is noted that under operation the sapphire surface of the μLED can heat up to above 50 °C if no thermal management approach is implemented. Here, no significant effect is seen on the CQD converter performance when integrated with the μLED, although no detailed study of the characteristics with temperature and prolonged operation is reported.

A. μLED-Based VLC Link

We demonstrate a free-space VLC link using a μLED hybridized with the CQD/PMMA color converters (Fig. 1(a)) as the optical source. The μLED is modulated with the encoded data. The blue μLED light is color-converted by the integrated CQD structure, which translates the modulated waveform to a green, yellow/orange or red optical carrier. A set of optics is used to collect the light and focus it onto an avalanche photodiode (APD, Hamamatsu S8664-05k) or a low noise Positive-Intrinsic-Negative photodiode (New Focus 1601AC). An optical filter is placed before the detection to filter the few percent of unabsorbed, as well as scattered, blue light. As a result, the detected optical signal is then only the color-converted waveform. In one of our tests, the filter is removed, in which case the detected light from the hybrid μLED is a combination of both converted and unconverted light. The overall distance between the hybrid μLED and the photodetector is 10 cm in these experiments. The received signal is recorded with an oscilloscope (MSO7104B), and processed offline with a MATLAB script. The received signal is Fast Fourier Transformed (FFT) and post-equalized before demodulation.

B. Orthogonal Frequency Division Multiplexing (OFDM)

OFDM is a multi-carrier modulation scheme that enables the efficient use of the bandwidth of an optical source, even past its modulation bandwidth. It is an attractive modulation scheme for high data rate VLC where non-linear signal distortion and inter-symbol interference can become an issue [19], [30]. Data streams are sent in parallel via orthogonal frequency subcarriers that are basically separated bands distributed over the bandwidth of the optical channel. In our case, each sub-carrier is modulated using multi-level quadrature (M-QAM) and the sub-carrier spacing is equal to a multiple of the M-QAM symbol duration. Adaptive bit and power loading is used so that the overall bandwidth utilization is maximized and enhanced performance is achieved. The power of the M-QAM symbols and the constellation size are adaptively allocated to each sub-carrier. The modulated sub-carriers are multiplexed in the time domain by inverse fast Fourier transform and digital-to-analogue conversion. Hermitian symmetry is imposed onto the OFDM signal, which is further DC-biased (DCO-OFDM) to ensure it is unipolar (only positive) and real-valued. The conditions are chosen so that the ODFM signal modulates the μLED as close as possible to the linear region of its optical power vs driving current characteristics, with the output power at the bias-point being 5 mW (4.5 V bias voltage).

The OFDM signal is generated, and the associated signal processing is done, using MATLAB. An arbitrary waveform generator (Agilent 81180A) is used to drive the μLED with the OFDM signal. A bias-T (ZFBT-4R2GW) enables DC-biasing.

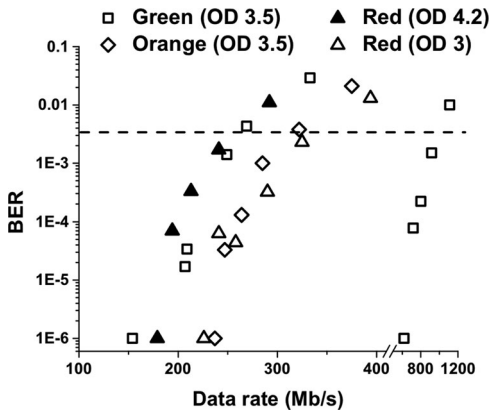

Fig. 8. BER versus data rate for different CQD/PMMA color converter samples integrated onto a μLED. The samples are identified by their OD values. All data are taken while detecting color-converted light only except for the open squares on the right that correspond to the light from the green CQD sample and the unabsorbed μLED light.

C. VLC Results

A total of four CQD/PMMA color converters were made and tested in the VLC link: one green sample (OD 3.5), one yellow-orange sample (OD 3.5) and two red samples (OD 3 and OD 4.2).

Fig. 8 plots the bit error rate (BER) versus the data rates for all these samples. The dashed line represents the BER value of 3.8 x 10^{-3}, which is the typical BER threshold if forward error correction is implemented. The data rate is determined by extrapolating the measurements to obtain such BER.

Data rates above 250 Mb/s are obtained for all the samples. 315 Mb/s and 345 Mb/s is obtained for the yellow/orange and the red (OD 3) samples respectively. The lowest data rate is for the green sample at 260 Mb/s. A combination of detection sensitivity, color converted power and modulation bandwidth explains these results. The red sample (OD 3) has the highest bandwidth while the orange and green samples have a lower bandwidth but convert more power. The spectral sensitivity of the silicon detector is also higher in the red and decreases monolithically as the wavelength decreases. We can see that the red sample OD 4.2 does not perform as well with data rate up to 265 Mb/s, similar to the green CQDs. This decrease in data rate compared to the red OD 3 sample is expected because at high OD both the converted power and the bandwidth are lower.

VLC at several hundreds of Mb/s is therefore readily achieved with a CQD-converted μLED. The performance of the VLC link is dependent on the detected converted power, which could be enhanced by adding a few simple features to the color converting structures. The slab geometry of the color-converters utilized here is not ideal for light-extraction as a non-negligible amount of light is trapped within the structure. Texturing the surface or shaping the CQD color converter, e.g. as a lens, can be done to obtain higher converted optical powers. Also, in our experiments, at least half the converted optical power is not detected as it is emitted towards the μLED and not in the detector direction. Adding a dichroic reflector on the backside of the color converter is therefore also a way to increase the detected converted power and hence the data rate. Because such performance is obtained at three different colors, and because the emission linewidth of CQDs is relatively narrow, coarse wavelength division multiplexing should be possible and offers another route to increase the data rates past the 1 Gb/s mark. We note that there is no specific thermal management approach for the μLED

Finally, the experiments described above are obtained by detecting *only* the color-converted light. In some application, for example illumination by color mixing, the color-converted light is mixed with the unabsorbed blue excitation light. In such a case, we can capitalize on this blue wavelength component to extend the VLC performance beyond 1 Gb/s simply by using an unfiltered hybrid color-converted μLED. This is shown in Fig. 8 for the green CQD-converted μLED. By removing the filter prior to the detector, unabsorbed excitation light is collected by the photodiode. In this particular case, 40% of the detected light is from the μLED and 60% from the green CQD/PMMA color converter. With such a hybrid source, the data rate is above 1 Gb/s.

V. Outlook

We have demonstrated a point-to-point VLC link using a CQD-converted μLED and discussed the performance of CQDs for this function and the parameters that can affect this performance. We have mentioned the potential for wavelength division multiplexing and an obvious next step is to study this capability. We note that although we reported here one format of color-converter (CQD/PMMA slab), we are also studying other formats of devices. These other formats as well as their high photostability operation will be reported elsewhere.

The performance of a VLC link is intrinsically dependent on the source modulation bandwidth and on the optical power received at the detector. From a color conversion aspect, it means high power conversion efficiency and a short PL lifetime are needed. Therefore, the focus should be on maximizing the radiative lifetime and on minimizing self-absorption. The colloidal CdSSe/ZnS heterostuctures utilized in this paper have a PL lifetime in the range of 10 to several 10's of ns limited by the fine structure of the exciton ground state. Therefore, even by minimizing self-absorption, the achievable modulation bandwidth with this material is unlikely to surpass 20 to 30 MHz. Apart from engineering the color-converters for optimization of the converted power as discussed above other types of colloidal materials can be considered.

One very promising class material is colloidal nanoplatelets (NPs) [31]. NPs are 2D atomically-flat colloidal materials with exciton confinement only in the vertical direction as opposed to three dimensions in CQDs. Because of their wide surface area, NPs have high oscillator strength, meaning that they have potentially faster PL lifetimes than CQDs. In addition, they have narrower emission linewidth, around 10 nm, which can enable the implementation of wavelength division multiplexing with more channels.

Perovskite QDs is also an emerging colloidal material that is being explored for photovoltaic, laser and color-conversion applications [32]. Some reported perovskite QDs have faster PL dynamics than chalcogenide CQDs and the PL linewidth is typically narrower. However this material system is still in its

infancy and much needs to be studied to confirm perovskite QDs as a possible contender for VLC.

VI. Conclusion

In summary, we have discussed CQD for light conversion of InGaN sources in VLC applications. We have explained the main characteristics relevant for a VLC color-converter. We have described how self-absorption can affect the emitted spectrum as well as the modulation bandwidth of CQD color converters, using a simple model that enables qualitative predictions. We have then reported the experimental characterization of chalcogenide CQD color-converter for green, yellow/orange and red emission. The trends and design guidelines identified in Section II were confirmed. These color-converters were then hybridized with a μLED and such a hybrid source was utilized to demonstrate free-space VLC over 10 cm at data rates up to 1 Gb/s. Finally, possible pathways to higher performance and alternative inorganic semiconductor colloidal materials were highlighted.

References

[1] J. Y. Kim, O. Voznyy, D. Zhitomirsky, and E. H. Sargent, "25th anniversary article: Colloidal quantum dot materials and devices: A quarter-century of advances," *Adv. Mater.*, vol. 25, pp. 4986–5010, 2013.

[2] I. L. Medintz, H. T. Uyeda, E. R. Goldman, and H. Mattoussi, "Quantum dot bioconjugates for imaging, labelling and sensing," *Nat. Mater.*, vol. 4, no. 6, pp. 435–446, Jun. 2005.

[3] T.-H. Kim *et al.*, "Full-colour quantum dot displays fabricated by transfer printing," *Nature Photon.*, vol. 5, pp. 176–182, 2011.

[4] V. I. Klimov *et al.*, "Optical gain and stimulated emission in nanocrystal quantum dots," *Science*, vol. 290, no. 5490, pp. 314–317, 2000.

[5] C. Dang *et al.*, "Red, green and blue lasing enabled by single-exciton gain in colloidal quantum dot films," *Nat. Nanotechnol.*, vol. 7, no. 5, pp. 335–339, 2012.

[6] B. Guilhabert *et al.*, "Nanosecond colloidal quantum dot lasers for sensing," *Opt. Express*, vol. 22, no. 6, pp. 7308–7319, 2014.

[7] D. Vasudevan, R. R. Gaddam, A. Trinchi, and I. Cole, "Core-shell quantum dots: Properties and applications," *J. Alloys Compounds*, vol. 635, pp. 395–404, 2015.

[8] T. Erdem and H. V. Demir, "Colloidal nanocrystals for quality lighting and displays: Milestones and recent developments," *Nanophotonics*, vol. 5, no. 1, pp. 74–95, 2016.

[9] S. Nizamoglu, G. Zengin, and H. V. Demir, "Color-converting combinations of nanocrystal emitters for warm-white light generation with high color rendering index," *Appl. Phys. Lett.*, vol. 92, 2008, Art. no. 031102.

[10] H. V. Demir *et al.*, "Quantum dot integrated LEDs using photonic and excitonic color conversion," *Nano Today*, vol. 6, no. 6, pp. 632–647, 2011.

[11] B. Guilhabert *et al.*, "Integration by self-aligned writing of nanocrystal/epoxy composites on InGaN micro-pixelated light-emitting diodes," *Opt. Express*, vol. 16, no. 23, pp. 18933–18941, 2008.

[12] N. Laurand *et al.*, "Colloidal quantum dot nanocomposites for visible wavelenght conversion of modulated optical signals," *Opt. Mater. Express*, vol. 2, no. 3, pp. 250–260, 2012.

[13] H. X. Zhang *et al.*, "Individually-addressable flip-chip AlInGaN micropixelated light emitting diode arrays with high continuous and nanosecond output power," *Opt. Express*, vol. 16, no. 13, pp. 9918–9926, 2008.

[14] J. Herrnsdorf *et al.*, "Micro-LED pumped polymer laser: A discussion of future pump sources for organic lasers," *Laser Photon. Rev.*, vol. 7, pp. 1065–1078, 2013.

[15] J. McKendry *et al.*, "High speed visible light communications using individual pixels in a micro light-emitting diode array," *IEEE Photon. Technol. Lett.*, vol. 22, no. 18, pp. 1346–1348, Sep. 2010.

[16] M. R. Krames *et al.*, "Status and future of high-power light-emitting diodes for solid-state lighting," *J. Disp. Technol.*, vol. 3., no. 2, pp. 160–175, 2007.

[17] R. X. Ferreira *et al.*, "High bandwidth GaN-based micro-LEDs for multi-Gb/s visible light communications," *IEEE Photon. Technol. Lett.*, vol. 28, no. 19, pp. 2023–2026, Oct. 2016.

[18] S. Rajbhandari *et al.*, "A review of gallium nitride LEDs for multi-gigabit-per-second visible light data communications," *Semicond. Sci. Technol.*, vol. 32, 2017, Art. no. 023001.

[19] H. Haas, L. Yin, Y. Wang, and C. Chen, "What is lifi?," *J. Lightw. Technol.*, vol. 34, no. 6, pp. 1533–1544, Mar. 2015.

[20] H. Haas, "A light-connected world," *Phys. World*, vol. 29, no. 8, pp. 30–34, 2016.

[21] D. C. O'Brien *et al.*, "Visible light communications: Challenges and possibilities," in *Proc. IEEE 19th Int. Symp. Pers. Indoor Mob. Radio Commun.*, 2008, pp. 1–5.

[22] F. Todescato *et al.*, "Engineering of semiconductor nanocrystals for light emitting applications," *Materials*, vol. 9, 2016, Art. no. 672, doi: 10.3390/ma9080672.

[23] M. Jones, S. S. Lo, and G. D. Scholes, "Quantitative modeling of the role of surface traps in CdSe/CdS/ZnS nanocrystal photoluminescence decay dynamics," *PNAS*, vol. 106, no. 9, pp. 3011–3016, 2009.

[24] U. Woggon *Optical Properties of Semiconductor Quantum Dots*. New York, NY, USA: Springer, 1997.

[25] A. P. Piquette, M. E. Hannah, and K. C. Mishra, "An investigation of self-absorption and corresponding spectral shift in phosphors," *ECS Trans.*, vol. 41, no. 37, pp. 1–9, 2012.

[26] T. Hao and R. E. Riman, "Calculation of interparticle spacing in colloidal systems," *J. Colloid Interface Sci.*, vol. 297, pp. 374–377, 2006.

[27] P. Asbeck, "Self-absorption effects on the radiative lifetime in GaAs-GaAlAs double heterostructures," *J. Appl. Phys.*, vol. 48, pp. 820–822, 1977.

[28] Z. Gong *et al.*, "Size-dependent light output, spectral shift, and self-heating of 400 nm InGaN light-emitting diodes," *J. Appl. Phys.*, vol. 107, no. 1, 2010, Art. no. 013103.

[29] M. S. Islim *et al.*, "Towards 10 Gb/s orthogonal frequency division multiplexing-based visible light communication using a GaN violet micro-LED," *Photonics Research*, vol. 5, no. 2, A35, Apr. 2017.

[30] M. S. Islim and H. Haas, "Modulation techniques for li-fi," *ZTE Commun.*, vol. 14, no. 2, pp. 29–40, Apr. 2016.

[31] S. Ithurria *et al.*, "Colloidal nanoplatelets with two-dimensional electronic structure," *Nat. Mater.*, vol. 10, no. 12, pp. 936–941, 2011.

[32] S. Yakinin *et al.*, "Low-threshold amplified spontaneous emission and lasing from colloidal nanocrystals of caesium lead halide perovskites," *Nature Commun.*, vol. 6, 2015, Art. no. 8056.

Miguel F. Leitao received the M.Sc. degree in physics engineering from Instituto Superior Técnico, Universidade Técnica de Lisboa, Lisboa, Portugal in 2013. He is currently working toward the Ph.D. degree in fast color converting materials at the Institute of Photonics, University of Strathclyde, Glasgow, U.K.

Joao M. M. Santos received the Ph.D. degree in physics from the Institute of Photonics, University of Strathclyde, Glasgow, U.K., in 2017. He is currently with ST Microelectronics, Edinburgh, U.K. His research interests include semiconductor detectors, optical sources, telecommunications, and optics.

Benoit Guilhabert received the Ph.D. degree in applied physics from the University of Strathclyde, Glasgow, U.K., in 2008. He is currently a Researcher with the Institute of Photonics, University of Strathclyde.

Scott Watson received the Ph.D. degree from the University of Glasgow, Glasgow, U.K., in 2016. He is currently working as a Postdoctoral Researcher in the optoelectronics group at the University of Glasgow. His main research interest includes optical wireless communications.

Anthony E. Kelly's, received the Ph.D. degree from the University of Strathclyde, Glasgow, U.K. He was with the British Telecom Laboratories and Corning. He was also a Co-Founder of Kamelian Ltd., Oxfordshire, U.K., and Amphotonix Ltd., Glasgow. He is currently with the School of Engineering, University of Glasgow. He has authored or co-authored more than 150 journal and conference papers on a range of optoelectronic devices and systems and holds a number of patents. His current research interests include semiconductor optical amplifiers and related devices, visible light communications using GaN devices, and high-speed lasers for PON systems.

Mohamed S. Islim (S'07) received M.Sc. (Distinction) degree in signal processing and communications from the University of Edinburgh, Edinburgh, U.K., in 2014. He is currently working toward the Ph.D. degree at Li-Fi R&D Centre, University of Edinburgh. He received the Global Edinburgh Syrian Scholarship from the University of Edinburgh in 2013, and the IEEE Communications Chapter Best Master Project Prize in 2014. His research interests include optical OFDM, Li-Fi, and optical wireless communications.

Harald Haas received the Ph.D. degree from the University of Edinburgh, Edinburgh, U.K., in 2001. He currently holds the Chair of Mobile Communications at the University of Edinburgh, and is cofounder and Chief Scientific Officer of pureLiFi Ltd., as well as the Director of the LiFi Research and Development Center, University of Edinburgh. His main research interests include optical wireless communications, hybrid optical wireless and RF communications, spatial modulation, and interference coordination in wireless networks. He first introduced and coined spatial modulation and LiFi.

Martin D. Dawson (M'85–SM'98–F'09) received the Ph.D. degree in physics from Imperial College, London, U.K., in 1985. He has worked at North Texas State University, Denton, TX, USA; the University of Iowa, IA, USA; Sharp Laboratories of Europe, Oxford, U.K.; and the University of Strathclyde, Glasgow, U.K. He is currently a Professor and the Director of research at the University of Strathclyde's Institute of Photonics, which he helped establish in 1996. Since 2012, he has been also the Head of the Fraunhofer Centre for Applied Photonics, Glasgow, U.K.

Nicolas Laurand (S'03–M'06) received the Ph.D. degree in applied physics from the University of Strathclyde, Glasgow, U.K., in 2006. He is currently an Associate Team Leader at the Department of Physics, Institute of Photonics, University of Strathclyde. His research interests include the optical properties of nanophotonic structures, including colloidal materials, developing novel hybrid materials and devices for healthcare, scientific instrumentation, and communications.